Engineering Failure Analysis 146 (2023) 107064

Contents lists available at ScienceDirect

Engineering Failure Analysis

journal homepage: www.elsevier.com/locate/engfailanal

Fatigue and failure analysis of aluminium and composite automotive wheel rims: Experimental and numerical investigation

Michele Zanchini [a], Daniel Longhi [a], Sara Mantovani [b,*], Francesco Puglisi [b], Mauro Giacalone [b]

[a] Ferrari S.p.A., Via Abetone Inferiore 4, 41053 Maranello, Italy
[b] Department of Engineering 'Enzo Ferrari', University of Modena and Reggio Emilia, Via Vivarelli, 10 41125 Modena, Italy

ARTICLE INFO

Keywords:
Automotive engineering
Automotive wheel
Aluminium alloys and composites
Forging and Resin Transfer Moulding
Finite element analysis and Mechanical testing
Fatigue
Manufacturing defects
Fail-safe design

ABSTRACT

This paper deals with the adoption of composites in the design of the wheel rims of a sports car. With particular reference to cornering structural performance, the design of a composite wheel rim, produced via Resin Transfer Moulding (RTM) led to a reduction in mass and to an increase in bending stiffness. The adoption of alternatives to aluminium alloys allows the unsprung masses, as well as the total mass of vehicle to be contained. This paper provides a comprehensive view of the fatigue tests used for the wheel rim type-approval, followed by a rundown of wheel rims designed by Ferrari S.p.A from 2009 to present. These wheel rims have been classified in terms of mass and stiffness, and manufacturing process like casting, forging, or RTM.

The failure modes of the reference Ferrari 488 GTB wheel rim were compared to those of the new composite wheel. In addition, the interpretation of the failures is supported by the results of Finite Element analyses. Though some initial defects led to a loss of stiffness of the wheel throughout the cornering fatigue test, the experimental results show that composite wheel rims are considered safe and they comply with the homologation targets and the Ferrari S.p.A. regulations.

1. Introduction

The whole concept of road vehicle lies on the presence of wheels between the vehicle body and the ground. Most of today's wheels present a series of spokes (spoke-type wheels) or a thin shell (disk-type wheels), which connect the rim to the central hub.

The main function of a wheel is to withstand the weight of the vehicle and the loads from the ground. Under service, a wheel is subjected to fatigue, to dynamic and impact loads [1,2]; a premature failure of a wheel could result in a sudden loss of the vehicle control by the driver. Therefore, three durability loading conditions are currently employed during the wheel design and testing, namely cornering fatigue, radial fatigue [3-7] and biaxial fatigue [8-10].

Cornering fatigue is largely dealt with in the literature, with contributions considering mechanical tests on spoke-type metal-wheels [11-13]. Ballo *et al.* [11] present a new design for an A356-T6 spoke-type wheel. After 3.5 million cycles, they find a crack at the root of one spoke, originating from the inner edge. A similar failure is found also in the work of Shang *et al.* [12]. The crack location is highly influenced by the wheel design. Raju *et al.* [13] experience a crack at the hub housing, close to the bolted holes. Adopting the stress-life

* Corresponding author.
E-mail address: sara.mantovani@unimore.it (S. Mantovani).

https://doi.org/10.1016/j.engfailanal.2023.107064
Received 18 November 2022; Received in revised form 24 December 2022; Accepted 13 January 2023
Available online 18 January 2023

(S-N) approach, Finite Element (FE) simulations of the fatigue test are developed to predict the critical spots in the wheel [11-14]. Some commonly adopted criteria include Sines and Matake [11], Goodman [12], and equivalent stress amplitude [14]. An alternative approach, proposed by Firat *et al.* [15] predicts the damage of the wheel with a strain life approach. The Fatemi-Socie parameter offers a good prediction of the fatigue resistance.

On accounting disk-type wheels, the literature provides contributions dealing with FE simulations [16-18] and experiments [19,20]. The critical spots in these wheels are the bolted holes [21], the ventilation holes [22-24] and to the welding seam between the disk and the rim [20,25].

The literature also presents studies on the radial fatigue of wheels. Raju *et al.* [26] discuss the numerical simulation and experimental test on an A356-T6 spoke wheel. Experiments show a crack originating at the root of one spoke, cutting the whole cross-section of the spoke. Once again, a S-N approach is adopted to estimate the fatigue life with numerical simulation. The results of the simulation are in close agreement with the experiments. Other contributions deal with the design and fatigue life prediction of steel disk-type wheels [23,25,27].

To increase the predictiveness of the simulations, the critical stresses need to be evaluated at every point of the wheel [10]; to have consistent data on the fatigue resistance of the material of the wheel, Kinstler samples some coupons directly from the wheel [2], the same is done by Ballo *et al.* [11], Raju *et al.* [13,26], and Archibald *et al.* [28].

Manufacturing and assembly have a non-secondary influence on the mechanical properties and fatigue strength of the wheels. Researchers investigate the effects of the rim interference fit [24,27], stamping [29] or punching [22] on disk-type wheels, as well as the post-casting solidification [30] on spoke-type wheels. The microstructure and the defects induced by manufacturing affect the overall fatigue resistance of the wheel as pointed out in [19,21,31].

The handling and the comfortable ride of a vehicle are enhanced by the reduction of the unsprung masses [32], among which wheels have a significant relevance. Furthermore, the reduction in the rotational inertia is effective in containing fuel consumption. In addition, the request for a constantly higher performance on the road or on the racetrack for new vehicles, let alone a possible increase in weight, has led to a general increase in the loads affecting the wheels under service.

To handle these higher forces, while giving wheels with a lightweight design, new wheels are designed with a combination of two approaches: material selection [33,34] and structural optimization. Optimization methods may be adopted to obtain a light rim with variable thickness [35,36] or the optimal topology of the spokes [37,38], as well as to enhance the vibration response [39] or the impact [40,41] resistance of the whole wheel.

Magnesium alloys are the lightest among the metals adopted for wheels, they also possess good formability; however, magnesium alloys exhibit a poor galvanic corrosion resistance and a low fatigue strength if compared to the aluminium ones. These characteristics make magnesium alloys a suitable choice for the design of motorsport wheels [33,40,41].

Recent advances in wheel design concern composite wheels. Composites have been introduced because of their high stiffness-to-weight ratio. SAE J3204 standard [42] distinguishes between *hybrid composite wheels*, in which metallic alloys and composites are present in either the rim or the spokes [39,41,43], and *composite wheels*, where both the rim and spokes are made in composite materials [37,44,45].

Rondina *et al.* [44] present a Carbon Fibre Reinforced Polymer (CFRP) wheel for sport cars produced from High-Pressure Resin Transfer Moulding (HP-RTM), which is promising to produce high volume rates. The authors analyse the detrimental effect of harsh environmental conditions on the CFRP mechanical properties and provide numerical simulations of the injection to minimise production time and defects.

Chai *et al.* [45] present a glass-fibre reinforced with polymer spoke wheel, manufactured via injection moulding. FE simulation of static bending reveal the most critical zones of the rim, which are confirmed by subsequent experiments. In their work, Chai *et al.* do not consider the prediction of the fatigue life of composite materials under multiaxial loads. This is in fact still a challenging topic in current research [46-49]. Fuji and Lin [50] observe that the S-N curves of a composite reinforced with glass fibres decreases with the compresence of tensile and shear loads. They use the S-N curve to tune the Tsai-Wu [51] failure criterion, obtaining a prediction of the composite failure after certain numbers of cycles.

The present paper aims to demonstrate that composites might be successfully adopted in wheel rim design. A purely composite wheel for a high-performance vehicle is presented. It consists of an inner preform obtained by a mixture of polymer matrix resin and chopped short carbon fibres, and of an outer stacking sequence produced by woven and unidirectional plies with long carbon fibres. The polymeric matrix is injected in the wheel with HP-RTM, as in [44].

The requirements of the type-approval standards and Ferrari S.p.A. protocols are compared for impact and fatigue tests. Then, a rundown of the wheel rims designed by Ferrari from 2009 to present, is provided. These wheel rims have been classified in terms of mass and stiffness, and manufacturing process like casting, forging for aluminium alloys, or RTM for composites.

The proposed composite wheel has been compared with a reference forged aluminium wheel. FE simulations have been performed to estimate the fatigue life of the wheels, adopting Dang Van [52,53] fatigue criterion for the aluminium wheel while the Tsai-Wu criterion was adopted for the composite one.

The wheels have been tested under cornering and radial fatigue. The two wheels satisfied the requirements of homologation standards and Ferrari protocols. The failure of the wheels after the fatigue tests have been analysed using non-destructive techniques like Computerised Tomography (CT) and dye penetrants.

2. Material and methods

The following subsections present the employed nomenclature, the most relevant experimental tests used for wheel homologation,

and an historical collection of sports car wheels. Furthermore, two wheels are considered as reference components for the failure analysis investigation: the first in aluminium alloy, and the second made of composites.

2.1. Wheel nomenclature

The terms *wheel* and *rim* are often used as synonyms; however, from a technical viewpoint, the term rim refers only to the outer thin shell, on which the tyre is mounted, while the wheel includes the wheel and its connection to the hub housing.

The tyre is radially positioned by means of two *beads*, and touches the extremity of the rim by pushing axially on two *flanges*. Rim flanges are classified by their shape, the commonest shape for passenger cars is the J-horn. The connection of the rim to the hub housing, which is made by a thin shell or by a series of spokes, divides wheels in disk wheels or spoke wheels, respectively.

A detailed view of a spoke wheel rim is provided in Fig. 1. It also shows a geometry of the hub housing, and the seat of the inflation valve. The inner distance between the flanges is called rim width (w). The nominal diameter (D) is the diameter of the beads. The offset (d) is the distance from the centre of the rim to the hub mating surface.

Fig. 1 shows candidate zones for the extraction of samples for the material fatigue life estimation, like the spokes (zone A), the rim flanges (zones B and C) and the hub housing region [11,26,28].

2.2. Type approval tests and requirements

Today's road vehicles are requested to keep a high comfort and safe handling over an increasing mileage. Furthermore, high performance vehicles require a precise dynamic performance over increasing speed. Under these circumstances, the fatigue endurance of the wheels must be addressed with care, in order not to harm the vehicle occupants during service. Five standard tests are mandatory for wheel delivery, which will be described in the following. The first two tests deal with the impact resistance of a wheel rim, while the third to fifth tests deal with the wheel's fatigue resistance. Table 1 lists these type approval tests, highlighting the standard

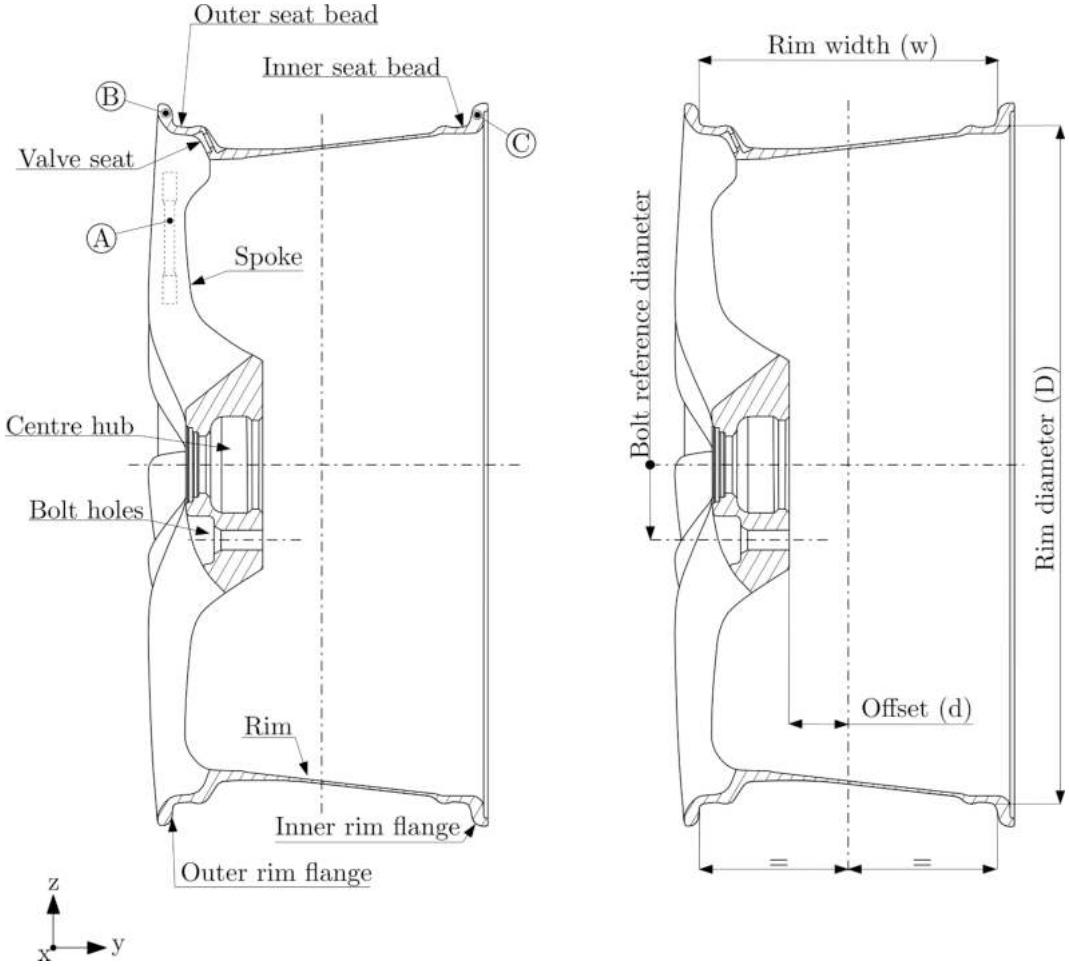

Fig. 1. Wheel rim nomenclature.

requirements for the wheels.

2.2.1. Impact tests

Two standard tests evaluate the wheel resilience facing either a lateral or a radial impact, which may occur when the wheel hits a bump, a pothole, or a sidewalk. In both these tests, the tyre is mounted on the wheel. In the lateral impact test [54], one front and one rear wheel (1 + 1) are inflated at the normal operating pressure. An impactor of peculiar size and shape drops on the side of the wheel from a height of 230 mm. The mass of the impactor M is expressed in kg as:

$$M = 0.6^{*}W + 180 \tag{1}$$

where W is the vehicle weight on the highest loaded axle. The impact occurs close to the outer rim flange, at 13 degrees from the

Table 1
Loading conditions and requirements for the main type approval tests.

Description	ID. Standard	Type-approval requirements	Ferrari requirements
Lateral Impact	SAE J175 (ISO 7141)	- No visible cracks - No spoke-rim separation - Pressure retained within 1 min after impact	Same as type-approval requirements
Radial Impact	AK-LH-08 for metal parts	Two different load stages. 1) At the first load level ($K = 1.15$), wheel deflection evaluated at the inner rim horn remains below a certain threshold. 2) At the second load level ($K = 4.3$), fracture not allowed except for: cracks at the impact area and cracks in deep-bed area up to 25% of periphery	Same as type-approval requirements De-beading is not permitted
Cornering Fatigue	SAE J328 (ISO 3006)	$\mu = 0.7$ Two load stages: $K = 2.00$ front wheel 1.75 rear wheel 50000 cycles - No fatigue crack penetrating through the section allowed - Wheel deflection within 20% of initial deflection	$\mu =$ from the project Two load stages: 1) $K = 2.00$ (both wheels) 250000 cycles 2) $K = 1.50$ (both wheels) 1000000 cycles - No crack allowed (dye penetrant test) - Wheel deflection below 10% of initial deflection - Wheel bolts tightening torque above 70% of original torque
Cornering Fatigue *(for Composite Wheels made of matrix material and fibre reinforcement)*	SAE J3204	$\mu = 0.7$ $K = 2.00$/SRFF front wheel 1.75/SRFF rear wheel 65000 cycles - No fatigue crack penetrating through the section allowed - Wheel deflection below 20% of initial deflection	$\mu =$ from the project Two load stages: 1) $K = 2.00$ both wheels 250000 cycles 2) $K = 1.50$ both wheels 1000000 cycles - No crack allowed (dye penetrant test) - Wheel deflection below 20% of initial deflection - Wheel bolts tightening torque above 70% of original torque
Radial Fatigue	SAE J328 (ISO 3006)	$K = 2.50$ front wheel 2.25 rear wheel 600000 cycles - No fatigue crack penetrating through the section allowed	$K = 2.5$ both wheels 1000000 cycles - No crack allowed
Radial Fatigue *(for Composite Wheels made of matrix material and fibre reinforcement)*	SAE J3204	$K = 2.50$/SRFF front wheel 2.25/SRFF rear wheel 750000 cycles - No fatigue crack penetrating through the section allowed	$K = 2.5$ both wheels 1000000 cycles - No crack allowed
Biaxial Fatigue	SAE J2562	Multiblock program based on specific load-cases reported into the protocol. - No loss of air pressure resulting from a fatigue cracks - No fatigue crack penetrating through the section allowed	Multiblock program based on specific customer requests. Other programmes: AKR multiblock cycle, Eurocycle LBF. Cracks are permitted as long as they do not compromise the wheel functionality and safety.

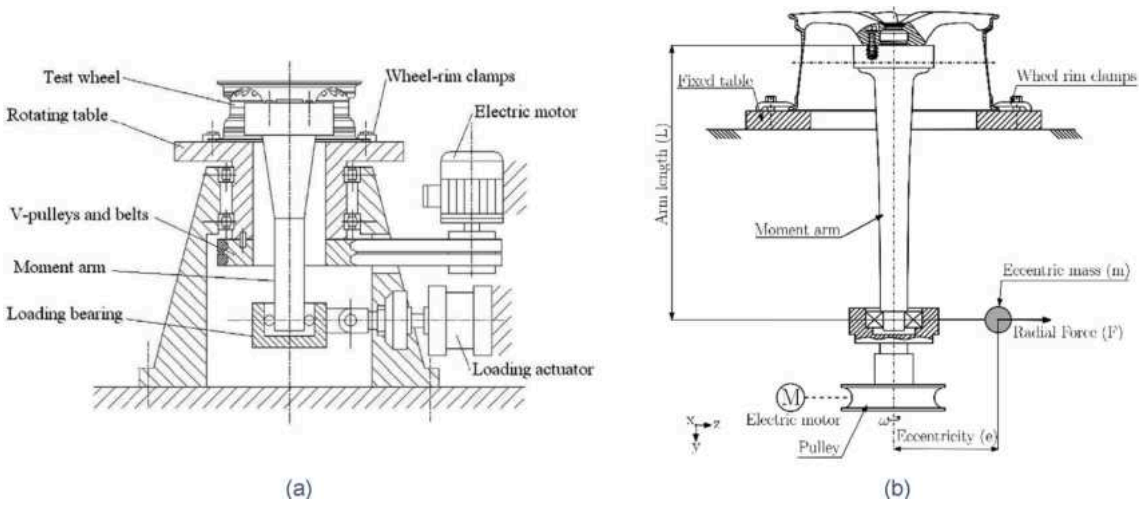

Fig. 2. Test rig layouts used for cornering fatigue test: a) with rotating table [13,17,39], b) with an eccentric mass [11,16,21].

wheel rotation axis. The test is passed, if no visible fractures are penetrating through the complete section of the wheel, if there is no separation between wheel centre and spokes or rim, and if the tyre pressure remains unaltered after 1 min from completing the test.

In the radial impact test [55], the tyre is impacted radially. For passenger cars, the tyre pressure is the minimum recommended by the manufacturer (e.g. 2.0 bar), and then impact energy E is evaluated by the following formula:

$$E = Kq \tag{2}$$

where K is an amplification factor, and q is the wheel load expressed in kg. Although, from the viewpoint of dimensional analysis, the above equation is inconsistent, it is adopted to correlate the fall height of the impactor to the impact energy and consequently to the impact speed. Six wheels (3 + 3) are impacted with V-shaped strikers [56,57]. The wheel is impacted twice. In the first impact K is set equal to 1.15, while in the second impact K is increased to 4.3. (see Table 1). At the lowest load, the test is passed if wheel deflection at the inner rim horn is below a certain threshold; then, at the second stage if cracks occur in the deep bed area that do not exceed 90 degrees (25%) of the periphery.

Impact tests are generally performed at the final stage of the wheel design. Therefore, failing one of these tests requires a wheel design revision which is time consuming and unprofitable. The literature presents various impact test simulations implemented to drive the wheel design, reducing thus the risk of failure [57-60]. In fact, to make the simulation more predictive, dedicated analysis on the striker shape, the wheel support structure, and the non-linear mechanical properties of the tyre, which mostly affect the outcome of the simulation, are explored [61].

2.2.2. Cornering fatigue test

This fatigue test simulates cornering forces by applying a rotating bending moment to the wheel. The inner rim flange is clamped to a table, and an arm is flanged to the hub. A force F is applied to the arm with a minimum distance of 762 mm (30 in) from the hub. This results in a prescribed bending moment applied to the hub. Two systems ensure that the bending moment rotates with respect to the wheel. In the first one (Fig. 2a) the plate rotates, while the force is applied by a fixed actuator [2]. In the second system (Fig. 2b), the

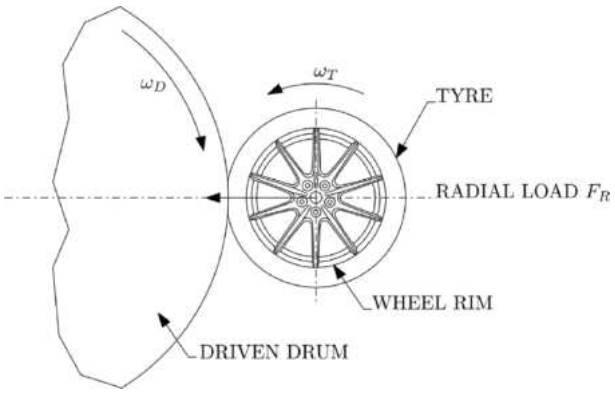

Fig. 3. Radial fatigue test setup. See also [2].

Table 2
Rundown of Ferrari wheel rims.

							FRONT				REAR			
Model	**Year**	**Powertrain**	**Style**	**No. spokes**	**Material**	**Technology**	**Dimensions** \vskip5\hfill \hbox\rot90{ \vskip5\hfill \hbox\rot90 { **[W × D]**	**Mass ratio**	**Design load ratio**	**Stiffness ratio**	**Dimensions** \vskip5\hfill \hbox\rot90{ \vskip5\hfill \hbox\rot90 { **[W × D]**	**Mass ratio**	**Design load ratio**	**Stiffness ratio**
458 Italia	2009	Rear-mid ICE		5	AlMg1SiCu 6061-T6	Forged + Flow-forming	8,5J × 20″	0.94	0.91	0.72	10,5J × 20″	1.04	1.20	0.95
458 Italia	2009	Rear-mid ICE		5	AlSi7Mg0.3 A356-T6	LPD Casting + Flow-forming	8,5J × 20″	1.13	0.98	1.01	10,5J × 20″	1.22	1.29	1.51
F12	2012	Front ICE		Multi spokes	AlSi1MgMn 6082-T6	Forged + Flow-forming	9,5J × 20″	0.89	1.09	0.82	11,5J × 20″	1.01	1.47	1.28
F12	2012	Front ICE		5	AlSi7Mg0.3 A356-T6	LPD Casting + Flow-forming	9,5J × 20″	1.22	1.10	1.33	11,5J × 20″	1.38	1.47	2.12
458 Speciale	2013	Rear-mid ICE		5	AlSi1MgMn 6082-T6	Forged + Flow-forming	9 J × 20″	0.83	0.90	0.59	11 J × 20″	0.91	1.23	0.96
458 Speciale A	2014	Rear-mid ICE		5	AlSi1MgMn 6082-T6	Forged + Flow-forming	9 J × 20″	0.86	0.90	0.67	11 J × 20″	0.96	1.23	1.11
488 GTB	2015	Rear-mid ICE		5	AlSi1MgMn 6082-T6	Forged + Flow-forming	**9 J × 20″**	**1.00**	**1.00**	**1.00**	11 J × 20″	1.02	1.26	1.28
488 GTB	2015	Rear-mid ICE		5	AlSi7Mg0.3 A356-T6	LPD Casting + Flow-forming	9 J × 20″	1.13	1.01	1.25	11 J × 20″	1.24	1.31	1.83
F12tdf	2015	Front ICE		10	AlMg1SiCu 6061-T6	Forged + Flow-forming	10 J × 20″	0.82	1.22	1.03	11,5J × 20″	0.90	1.54	1.46
812 Superfast	2017	Front ICE		Multi spokes	AlMg1SiCu 6061-T6	Forged + Flow-forming	10 J × 20″	0.95	1.25	1.11	11,5J × 20″	1.04	1.58	1.45
812 Superfast	2017	Front ICE		5	AlSi7Mg0.3 A356-T6	LPD Casting + Flow-forming	10 J × 20″	1.22	1.25	1.46	11,5J × 20″	1.38	1.58	2.29
488 Pista	2018	Rear-mid ICE		10	AlMg1SiCu 6061-T6	Forged + Flow-forming	9 J × 20″	0.83	1.04	1.07	11 J × 20″	0.93	1.34	1.58
488 Pista	2018	Rear-mid ICE		10	CFRP	Preformed hand layup + RTM	9 J × 20″	0.72	1.10	0.95	11 J × 20″	0.76	1.46	1.08
488 Pista Spider	2019	Rear-mid ICE		Multi spokes	AlSi1MgMn 6082-T6	Forged + Flow-forming	9 J × 20″	0.98	1.03	1.24	11 J × 20″	1.07	1.38	1.83

(*continued on next page*)

Table 2 (*continued*)

							FRONT				REAR			
Model	**Year**	**Powertrain**	**Style**	**No. spokes**	**Material**	**Technology**	**Dimensions [W × D]**	**Mass ratio**	**Design load ratio**	**Stiffness ratio**	**Dimensions [W × D]**	**Mass ratio**	**Design load ratio**	**Stiffness ratio**
F8 Tributo	2019	Rear-mid ICE		Multi spokes	AlSi1MgMn 6082-T6	Forged + Flow-forming	9 J × 20″	1.04	1.04	1.09	11 J × 20″	1.12	1.34	1.32
812 GTS	2020	Front ICE		10	AlMg1SiCu 6061-T6	Forged + Flow-forming	10 J × 20″	1.02	1.30	1.39	11,5J × 20″	1.09	1.62	1.67
SF90 Stradale	2020	PHEV*		5	AlSi1MgMn 6082-T6	Forged + Flow-forming	9,5J × 20″	1.14	1.25	1.34	11,5J × 20″	1.24	1.55	1.97
SF90 Stradale	2020	PHEV*		5	AlSi7Mg0.3 A356-T6	LPD Casting + Flow-forming	9,5J × 20″	1.31	1.25	1.79	11,5J × 20″	1.45	1.55	2.26
SF90 Stradale	2020	PHEV*		10	CFRP	Preformed hand layup + RTM	9,5J × 20″	0.79	1.33	1.34	11,5J × 20″	0.85	1.56	1.64
812 Competizione	2021	Front ICE		10	AlSi1MgMn 6082-T6	Rotary forging + Flow-forming	10 J × 20″	1.00	1.29	1.10	11,5J × 20″	1.13	1.76	1.60
812 Competizione	2021	Front ICE		10	CFRP	Preformed hand layup + RTM	10 J × 20″	0.79	1.29	1.40	11,5J × 20″	0.82	1.76	1.49

wheel is fixed, and F is the centrifugal force of an eccentric mass, rotating around the arm's free extremity.

Grubisic et al. [10] critically discuss the effect of clamping on the load transfer and on the wheel deformation for a tested wheel and the same wheel under an actual cornering manoeuvre. In 2021, Anandraj et al. [36] present an innovative setup which also includes part of the suspension system for an actual dynamic loading condition. The natural frequencies of the rotating shaft might be monitored to avoid any vibration issue, as reported by Wang et al. [17].

The maximum reference bending moment at the wheel hub is determined as:

$$M = KWg(\frac{\mu D}{2} + d) \tag{3}$$

where W is the vehicle weight on the highest loaded axle, μ is the static friction coefficient, D is the diameter of the wheel and d is the wheel offset (see Fig. 1). K is an amplification factor adopted to accelerate the fatigue test, which would otherwise last 10^7 cycles to simulate the expected life of a wheel [16]. Values of K are given in the standard procedures and justified by Kinstler [2]. The force (or the eccentrical mass) is tuned to induce the moment M on the hub and in [3] the test is conducted at this reference bending moment M up to 50,000 cycles. In other standards and homologation protocols, as UN/ECE R124 [7], the test is conducted with two different levels of bending moment: the first level considers the 50% of the maximum bending moment M, while the second one considers the 75% of M. At least, two wheels (1 front and 1 rear) need to be tested at each level to fully comply with the standard.

According to SAE J328 [3], the test is passed if no fatigue cracks penetrating through the section are detected before the minimum required number of cycles, and if the deflection of the arm does not exceed 20% of the initial one. According to other more restrictive standards [4-6], no cracks must be detected using a non-destructive method, such as dye penetrants, on the wheel before a minimum number of cycles is reached. This number of cycles depends on the material of the wheel and the vehicle category. Furthermore, the test is successful, if the deflection of the arm does not exceed a certain threshold and if the tightening torque of the bolts remains above 70% of the initially applied torque, for details see Table 1.

2.2.3. *Radial fatigue test*

Radial fatigue test (or rim roll test) replicates the straight driving conditions of the wheel. The wheel is bolted on a test fixture which is representative of the actual wheel hub. The wheel rotates against a rigid-driven drum, which is kept in contact with the tyre by a hydraulic actuator, as in Fig. 3.

Being the rotation axes of the wheel and drum parallel, the test does not account for any camber angle occurring during normal driving conditions. Furthermore, the driven drum is almost smooth, so, the natural asperities of the road are neglected in this experimental protocol.

To accelerate the fatigue test, determining thus, a safe fatigue design of the rim, the tyre is inflated with a pressure (4.5 bar) higher than that in normal operating conditions (2.1 bar). The radial load (FR) imposed by the hydraulic actuator is increased by a factor Khigher than 1. The radial load of testing is expressed as:

$$FR = KWg \tag{4}$$

where K varies for front and rear wheels. For [3], the test is passed as for cornering fatigue if no fatigue cracks penetrating through the section are detected by a visual check and before 600000 cycles. Other standards require that no cracks are detected by dye

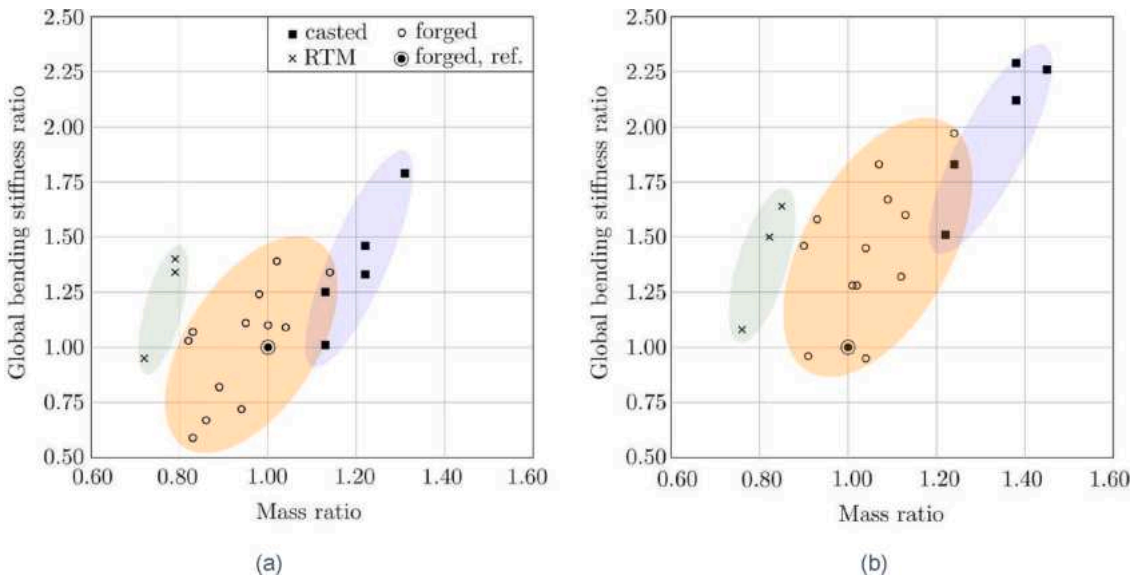

Fig. 4. Comparison of the global bending stiffness ratio on the mass ratio between families of a) front and b) rear wheel rims.

penetrants [7].

2.2.4. Biaxial fatigue test

The biaxial fatigue test aims to mimic normal driving conditions consistently [9,10,15]. To do so, the wheel is mounted to its actual spindle and is put in rotation against a driven drum, while two hydraulic actuators apply radial and lateral loads to the wheel [28].

Biaxial loads are derived from the load histories of the wheels under specific conditions, such as public roads or motorsport tracks like Nürburgring or Hockenheimring [28]. A survey of the experimental protocols and the numerical correlation methodology are reported by Wan et al [62] and by Santiciolli et al. [63].

2.2.5. Fatigue resistance requirements

Table 1 summarises the main features of the aforementioned tests, underlining the requirements from the international type approval standard. The commonest standards address wheel rims made up of metal alloys. A recent standard has been specifically developed to regulate the radial and lateral fatigue tests for aftermarket composite wheel rims [42]. In this standard, a parameter called SRFF is introduced: this is a fatigue reduction factor imposed by the wheel manufacturer to consider matrix performance reduction in ageing tests.

In the pursuit of a constant improvement of vehicle safety, Ferrari applies more challenging requirements to the wheels for the same approval tests. These requirements are placed besides the legal ones, see Table 1.

2.3. Ferrari wheel portfolio

Table 2 lists the wheels equipped in the sports cars manufactured by Ferrari in recent years. The collection of data details:

- Material of the wheel.
- Manufacturing process.
- Number of spokes.
- Width (w) and diameter (D) of the rims.
- Mass ratio of front and rear wheels.
- Design load ratio adopted to design the front and rear wheels.
- Stiffness ratio, measured from a quasi-static bending test of the front and rear wheels.

The last three quantities are scaled with respect to their counterparts on the front wheel mounted on the 488 GTB, which is taken as the reference.

So far, aluminium alloys are the commonest materials adopted in the design of automotive structural components, and wheels are no exception. Three alloys have been employed. Metal wheels are mostly forged or made up from low-pressure casting. Once the first step is concluded, a flow-forming is employed to give the rim its final shape.

During the years, vertical and lateral forces acting on wheels have gradually increased. This is mainly due to two reasons. The first one is the introduction of new systems in the vehicle, such as passive safety devices, hybrid drivelines, battery packs, which have increased the vehicle mass. The second reason is the improvements in aerodynamic downforce, which has allowed higher speed in corners. This has generally resulted in the adoption of progressively higher loads in wheel design.

Such loads may be handled by increasing the size of the wheels. In fact, through the years, the rim width has been gradually increased (see Table 2); however, the rim diameter has been kept equal to 20″. In fact, the wheel diameter usually depends on many factors like the aesthetic style, as well as, the size of the vehicle, and the expected driving performance.

To contain the mass of wider and wider rims, a progressive lightening of the hub housing and the bolted area has been obtained by means of numerical optimizations. This trend is evident by comparing the casted 458 Italia (2009) with the forged 812 Competizione (2021) wheel rim.

The optimization process has been also applied radially from the hub area towards the spoke periphery, to facilitate the brake cooling and to improve the melt flow of cast rims. In fact, the increase of top cruise speed has required careful thermal management of the wheel. This may be done by thinning the spokes, or by adopting dedicated ventilation wings on the spokes [64]. These wings also positively improve the aerodynamic efficiency of the vehicle, see SF90 Stradale.

In addition, Table 2 points out the number of spokes per each wheel. These are gradually increased from 5 to 10 during the years, apart from the F12tdf (2015) and 488 Pista (2018). This design aspect is mainly ascribable to aesthetic targets; furthermore, this choice ensures a uniform distribution of the operating loads.

Optimization techniques allowed the design of aluminium rims which bear loads up to 75% higher than that of the reference rim. However, this has led to an increase in the mass of newer wheels, up to 45% more than the reference. For a further weight reduction of the vehicle components, composite materials were introduced on wheel design, leading to three wheel rims (488 Pista in 2019, SF90 Stradale in 2020, 812 Competizione in 2021) which are lighter than the forged reference one. The RTM manufacturing process has been selected for the production of these wheels.

Fig. 4 shows a more comprehensive view of the effects of the material selection and of the manufacturing process on the global bending stiffness and on the normalised mass. Each bubble encloses a manufacturing process. The rear wheels present a higher bending stiffness ratio than the front ones. For the same value of the bending stiffness, the forged aluminium wheels exhibit lighter design, if compared to the casted parts. Composite wheels represent a promising alternative to the traditional metal alloys, since their adoption

may achieve a weight reduction of the component, together with a fairly high bending stiffness. In fact, the Resin Transfer Moulding wheel design, highlighted by the green area, is located at the left of forged technology.

2.4. Carbon wheel concept

The first composite wheel rim designed by Ferrari was presented in 2018, as an optional product for the 488 Pista. Numerical and experimental tests on this wheel will be described in the following.

The wheel consists in an inner preform obtained from randomly distributed milled fibres and a polymeric foam. Unidirectional and fabric composites plies are stacked on the preform, then, the dry assembly is placed within a mould. Afterwards, Resin Transfer Moulding (RTM) begins; resin is injected at a prescribed pressure, while a prescribed temperature cycle ensures the matrix polymerization. This process is most promising for high volume rates of parts with high geometrical complexity, as pointed out by Rondina et al. [44].

Fig. 5.a and 5.b show the global views of the composite wheel, while Fig. 5.c and 5.d detail the hub housing and the bolted areas.

According to SAE J3204 [42], the wheel presented in this work may be classified as a composite wheel. Nevertheless, metal alloys, up to 6% of the mass of the wheel, are employed to connect the wheel to the car. An aluminium backplate is placed at the contact interface between the wheel and the hub, to avoid excessive wear of the composite [21,36]. The backplate also helps the centering of the wheel, avoiding any possible imbalance. Additional metal inserts are placed at the internal surface of the bolted holes, to preserve the initial tightening of the bolts, see Fig. 5.d.

The bill of materials is reported in Fig. 6. UniDirectional (UD) carbon fibres and epoxy resin contribute to the 54% and the 25% of the overall mass of the wheel, respectively. The volume fraction of the UD fibres ranges between 55 and 60%.

The plain weave carbon fibre fabric is manufactured by PolyAcryloNitrile fibres, it is placed at the outer surface of the part for aesthetic purposes. This material covers the 4% of total mass of the part.

The internal preform, consisting in milled carbon fibres embedded into epoxy resin and polymeric foam, helps the manufacturing process. It acts like the honeycomb core of sandwich panels. In fact, its main purpose is to keep the structural UD laminates distanced from each other, thus increasing the overall stiffness of the spokes.

Finally, Non-Structural Mass (NSM) gathers all constituent materials that do not have a significant influence on the structural performance of the wheel rim, such as the inner ceramic thermal coating and the gloss paint.

Fig. 5. Composite wheel concept of 488 Pista: global and detailed views from the inside (a, c) and outside (b, d).

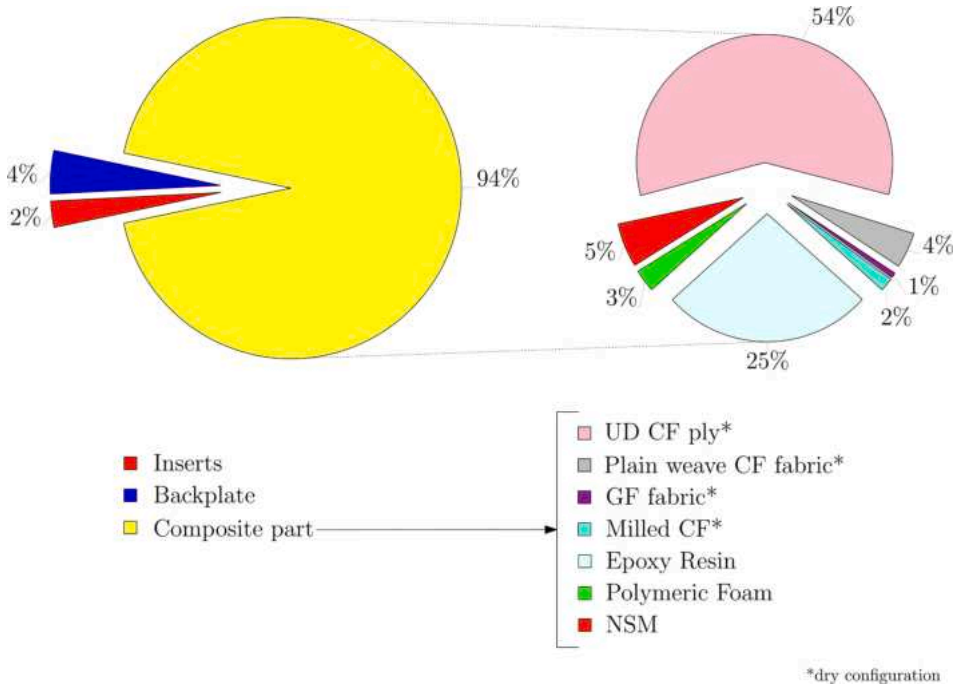

Fig. 6. Mass distribution of the 488 Pista composite front wheel.

After the 488 Pista composite wheel, two more composite wheels were designed (see Table 2) with slight changes in the spoke shape and the preform composition. These changes induced a higher stiffness in these wheels. Furthermore, it is also noted that the width of the newer composite wheels increased from 9 J to 10 J for the front rim, and from 11 J to 11.5 J for the rear one.

2.5. FE simulations

The stress field and the durability of the wheel rim have been investigated with the aid of FE methods. The models contribute to the development of useful design guidelines and their results have been compared with the experimental data. In the following, the model setup and the expected numerical outcomes have been reported for the simulations of cornering and radial fatigue tests. The commercial software ABAQUS has been employed in this study.

Fig. 7. Front wheel-tyre assembly of: (a) reference 488 GTB wheel forged in aluminium alloy; (b) 488 Pista in composite.

The reference aluminium wheel rim (Fig. 7.a) has been discretized by second-order tetrahedral elements (C3D10), the mesh size varying gradually from 5 mm to 1 mm. The minimum element size is located at the fillet radius between the spokes and the central hub housing, where previous contributions evidenced high failure probability [11-14]. In addition, a thin layer of quadratic, 6-noded shell elements (STRI65, thickness = 0.01 mm) has been built over the solid mesh to collect the stresses and strains for the fatigue evaluation.

The preform of the composite wheel rim (Fig. 7.b) has been discretized by first order tetrahedral elements (C3D4), adopting the same mesh size and refinement as the aluminium wheel rim. The CFRP laminates have been modelled with 8-noded hexahedral continuum shell elements, with reduced integration, hourglass control, and finite membrane strain (SC8R). The nodes of the shell elements coincide with the nodes of the preform. The backplate and the metal inserts, located at the bolted areas have been modelled by 8-noded hexahedral elements (C3D8R), assuming that they stick to the composite layers perfectly.

About 700000 and 500000 elements have been employed for the aluminium and the composite wheel rim, respectively. The materials are assumed to be linearly elastic: the aluminium alloy is isotropic, while an orthotropic law is adopted for the composite plies. Classical lamination theory has been used to determine the equivalent properties of the laminates.

Table 3 collects the mechanical properties employed for the aluminium alloy and for the constituents of the composite wheel rim. Dedicated experimental tests have been performed to retrieve the mechanical properties of the plain weave fabric and of the UD ply [65]. The properties of the remaining materials have been retrieved from the literature.

The two FE models underwent the simulation of a single cycle of each fatigue test. The multiaxial stress and strain state have been collected throughout the cycle and post-processed to obtain an estimation of the wheel's life expectancy for a complete load-revolution time history. The results will be presented in Section 3. The Dang Van criterion [52,53] for multiaxial high-cycle fatigue has been employed to compute the fatigue safety factor of the aluminium wheel.

Conversely, the estimation of the fatigue life of the composite wheel is on a different level of complexity. The Tsai-Wu criterion [51] has been used for the evaluation of the safety margin of the wheel. Inspired by the work made by Fuji and Lin [50], this work considers the stress limits derived from static stress on the composite. However, the results of the fatigue analyses on the composite wheels are to be considered as qualitative, they may be helpful in determining the critical zones in the wheel, but an accurate life estimation of the wheel requires further investigations.

2.5.1. *Cornering fatigue*

In the FE simulation of the cornering fatigue test, the tyre is neglected, see Fig. 8. The inner flange is fixed along its perimeter, and a multi-point constraint (RBE2) connects the centre hub housing to the loading point, which is 750 mm apart [14,29]. A concentrated force is applied to the loading point so that the resulting bending moment is equal to that applied in the experimental fatigue test and according to Equation (3) and Table 2.

The full fatigue cycle consists of 20 linear static simulations. Each simulation sees a load applied 18 degrees apart from the previous one. The stress fields have been then combined and processed to estimate the fatigue life of both wheels.

2.5.2. *Radial Fatigue*

The radial fatigue test within the virtual environment requires the complete wheel-tyre assembly, and proceeds with three subsequent nonlinear simulations:

1. interference fit between the tyre and the rim beads, according to the mounting protocol;
2. inflation of the tyre up to the operating pressure of 4.5 bar;
3. progressive contact between the driven drum and the tyre, induced by the radial force.

Table 3
Mechanical properties of the reinforcements, epoxy matrix and foam.

Material	E [MPa]	ρ [kg/m^3]	Refs.
Carbon Fibre for Plain weave Fabric	223000	1760	[66]
Standard Modulus Carbon Fibres with aesthetic properties			
Carbon Fibre for Plain weave Fabric and UD ply	240000	1800	[65]
Standard Modulus Carbon Fibres for structural performance			
E- Glass Fibre for Plain weave Fabric	72000	2540	[67]
Milled Carbon Fibre for the preform	10000 – 25000	800 – 1200	[68]
Epoxy resin for RTM process	2700	1170	Gurit Prime 180 [69]
Polymeric foam	36	32	Rohacell 31 IG-F [70]
Aluminium alloy	70000	2700	Inserts of composite wheel and casting and forged [71,72]

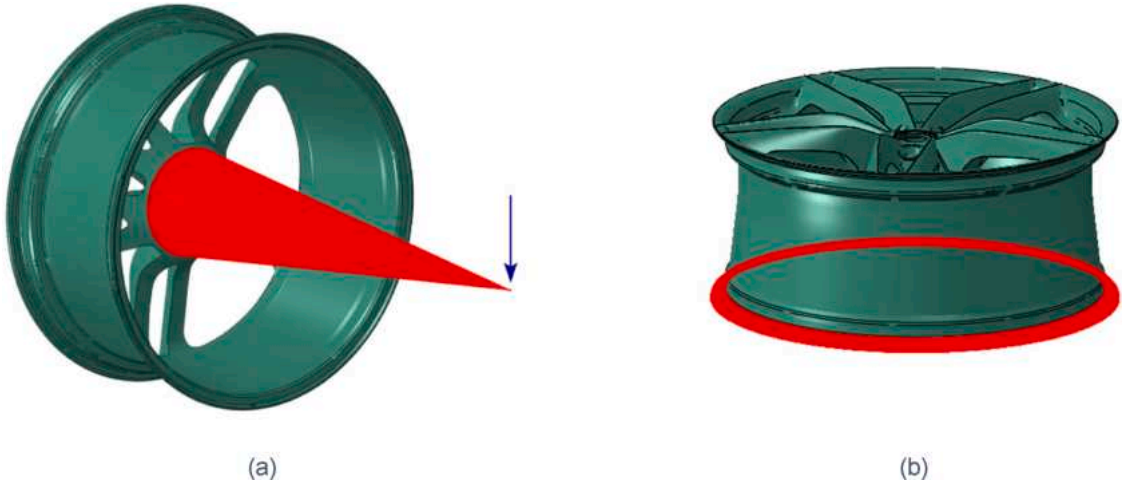

Fig. 8. FE model for cornering fatigue: a) RBE2 with load, and b) the fixed constraints at the inner flange.

The driven drum in the third simulation is modelled by a rigid plane in contact with the tyre in a prescribed position. Once again, the full rolling of the wheel on the driven drum is simulated by means of 20 simulations, where the drum is kept in contact with the tyre on a limited area. All the contact points are 18 degrees apart from the next ones, to span the whole 360 degrees evenly. The rigid plane is kept in contact with a force coherent with the actual experimental test and derived from Equation (4).

A friction coefficient of 1.3 is adopted for the contact between the tyre and the rigid plane, while the friction coefficient between the tyre and the rim flanges is set to 0.5 [73,74]. The rolling resistance of the tyre and the camber angle are omitted from these analyses. The composite and the aluminium alloys have been assumed to behave as linearly elastic. The material properties of the tyre and the numerical procedure used to model its nonlinear behaviour are retrieved from the literature [59]. The present simulations adopt the same mesh of the cornering fatigue simulations.

2.6. *Experimental testing*

Cornering and radial fatigue tests have been conducted on the forged aluminium front wheels of Ferrari 488 GTB, as well as on the composite wheel of Ferrari 488 Pista.

Cornering fatigue has been carried out as described in Section 2.2.2. The composite wheels have been tested using the turning table test rig (Fig. 2.a), while the aluminium wheels have been tested using the test rig equipped with the rotating eccentric mass (Fig. 2.b). In both cases, the overall bending stiffness of the wheels was collected throughout the tests. The same bending moment is applied to both wheels assuming that the testing layout does not affect the fatigue life estimation of the part.

The composite wheels underwent a non-destructive micro-Computerised Tomography (CT) analysis to check for the structural integrity of the preform and laminates. Four inspections have been made: 1) before the thermal coating spraying, 2) after 250000 cycles according to the Ferrari regulations, 3) when the wheel deflection was below 20% of initial deflection and, finally, 4) at 1 million cycles.

The fatigue test has been interrupted before each inspection. After the CT scan, the wheels have been mounted back on the test rig

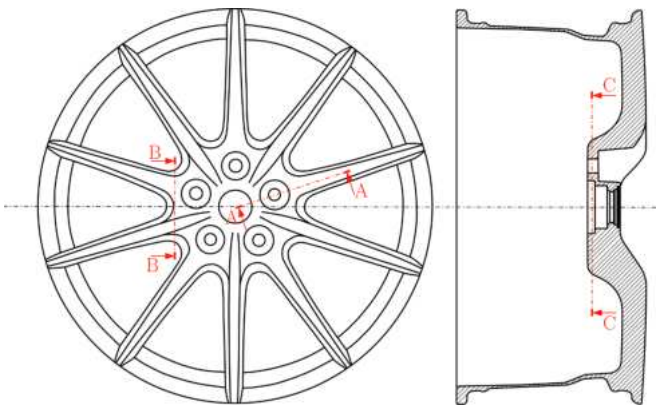

Fig. 9. Wheel cross-sections analysed by CT.

and the bolts have been tightened with the initial tightening torque.

The wheels have been examined on a North Star Imaging X5000 CT scanner to collect the internal damage occurrence and evolution. The voltage of the scanner has been set to 250 kV. The results on three significant sections of the wheel will be reported in the following. These sections, named as A-A, B-B and C–C, are shown in Fig. 9. The failure modes presented in the following summarised the recurrent damages and their evolution in composite wheels.

Radial fatigue tests have been carried out in accordance with the standard procedure shown in Section 2.2.3 [3,42]. The loads and duration of the tests have been chosen according to Ferrari regulations. After the test, the detection of damages has been revealed by visual inspection for the aluminium wheel, whereas the composite wheel has been checked with a dye penetrant test.

3. Results and discussion

Fig. 10 shows the results of a dye penetrant test on the composite wheel, performed after the radial fatigue test. The wheel does not exhibit any damage after 10^6 cycles, confirming that the wheel design is overconservative with respect to this fatigue test requirements.

Cornering fatigue tests are more critical for wheel designs; this section deals more extensively with the experimental results of these tests.

The reference aluminium wheels failed after about $7x10^6$ cycles. Up until that point, the bending stiffness decrease was negligible and in the order of 3%. Fig. 11 shows two different failures occurred to the two aluminium wheels, at the maximum load ($K = 2.0$) of the cornering fatigue tests. The failures are compared to their numerical counterparts. In the first case (Fig. 11.a), the crack originates from the front edge of a spoke, while in the second case (Fig. 11.c), the onset of the crack is found at one of the back edges of a spoke, close to the fillet. In both cases, the crack propagates through the spoke, until it cuts the whole cross section.

The two cracks originate at the section of maximum bending moment on the spoke. The main cause of the fatigue crack at the outer edge is the triangular cross-section of the spoke, which enhances the stresses in that zone. The second failure is also observed by Ballo et al. [11] and Shang et al. [12]. Here, the curvature of the spoke acts as a stress concentrator. The fatigue cracks most likely originate because of inner defects in the material, which may be reduced by tuning the number of punches, as well as their stroke and speed, even with the aid of simulations.

The layout of the wheel rim, as well as the cross-section of the spoke is a mandatory design input. Therefore, the onset of the crack at the outer edge of the spoke is inevitable, at some point. The FE simulations helped the dimensioning of the cross-section to extend the life of the wheel over a reasonable number of cycles. Fig. 11.b and 11.d report the life expectancy of the aluminium wheel resulting from FE analyses. The contour plot refers to the scalar factor called *Life* which returns, if multiplied by 250000, the number of cycles at which the failure occurs. The fundamental unit of 250000 cycles is chosen from the cornering fatigue tests legal requirements, to emphasise the over-conservativeness of the wheel design. This approach is alternative to what is proposed by [11,23], who report the number of expected cycles directly.

The minimum life of our aluminium wheels is above 19. Hence, the FE failure is expected after circa 4.9×10^6 cycles. Both wheels failed experimentally after about 7×10^6 cycles. Therefore, the FE simulations are 40% more conservative than the experiments. The numerical predictions seem to be overconservative, especially if compared with those of [26]. This inaccuracy is mainly due to preliminary characterization of the aluminium alloy under fatigue. Thus, the life prediction method may be refined by extracting additional samples from the wheel, obtaining a more accurate S-N curve. In any case, the life expectancy of the wheel numerically complies with the Ferrari requirements, enough to pave the way for fatigue wheel tests.

Fig. 12 shows the visual inspection of the composite wheel after 250000 cycles at the maximum level of loading. The wheel exhibits a superficial damage at the transition between two adjacent spokes (Fig. 12.a). Dye penetrant inspections (Fig. 12.b-c) evidence further cracks at the connection between the spoke and the rim. Here, the small fillet radius causes a significant stress concentration. It is worth to note that these damages are in resin-rich zones, and do not compromise the structural integrity of the wheel after 250000 cycles.

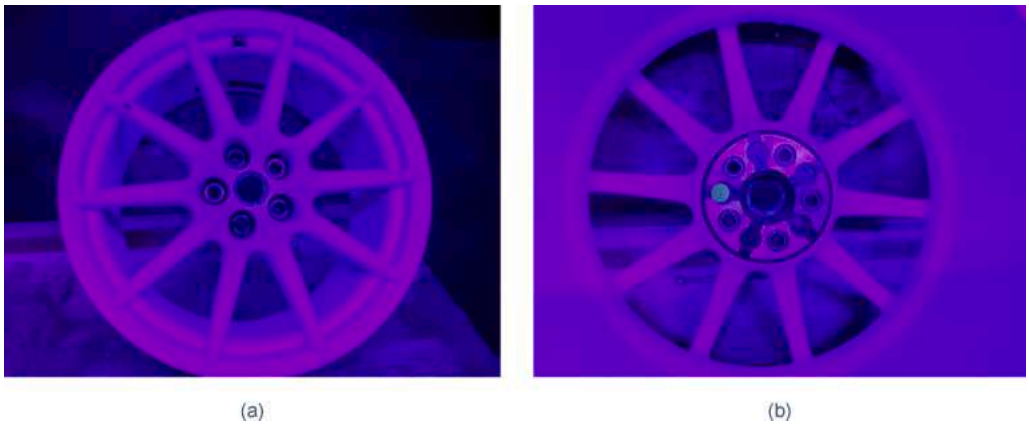

Fig. 10. Dye penetrant test on the composite wheel rim after the radial fatigue test: (a) outer and (b) inner views from the vehicle viewpoint.

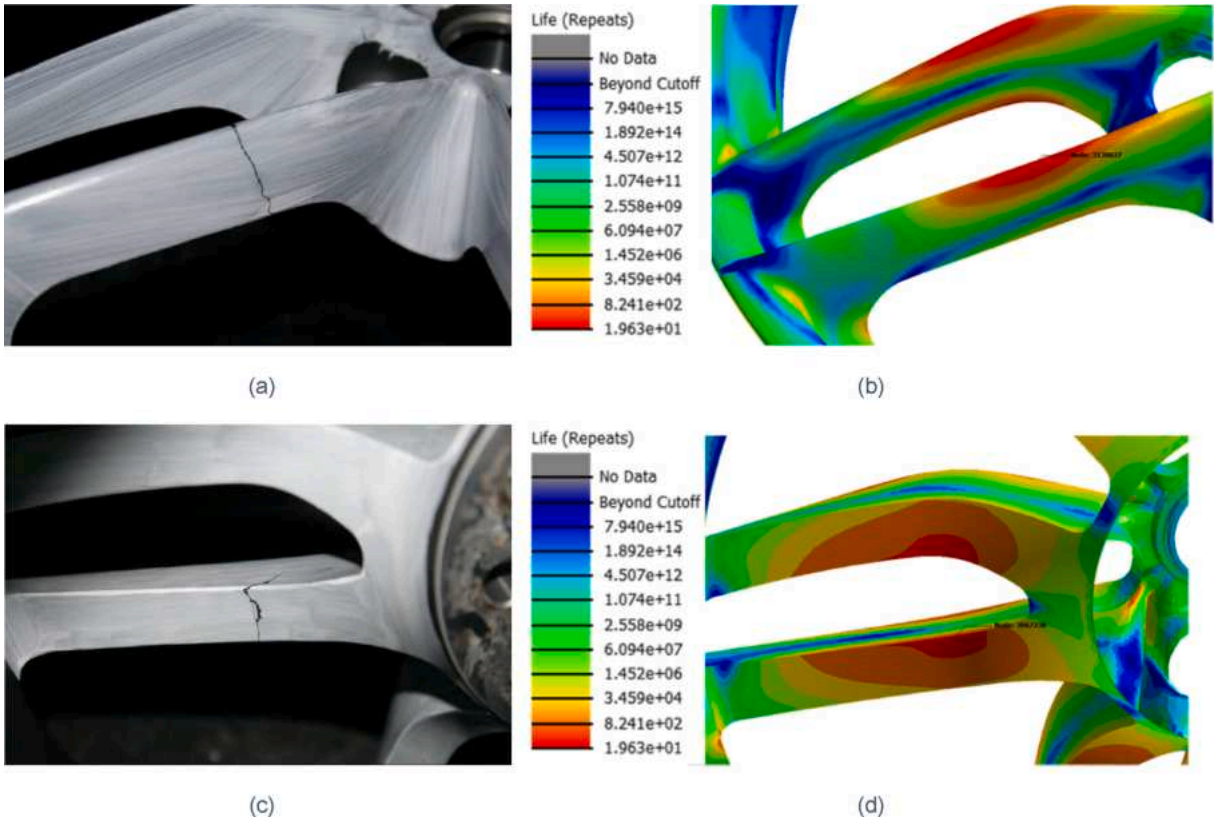

Fig. 11. Detailed views of aluminium front wheels of 488 GTB from the inner vehicle perspective (a, c), fatigue life expectation via FE (b, d).

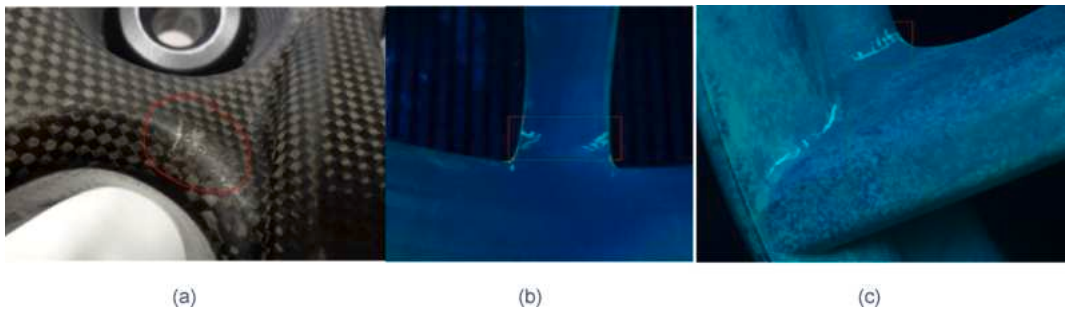

Fig. 12. Failure investigation after 250000 cycles under cornering loads: (a) at the radiused area between adjacent spokes, (b) and (c) dye penetrants results at the transition between a spoke and the rim.

As anticipated in Section 2.5, Tsai-Wu failure index was adopted to determine the most critical regions of the wheel. Fig. 13 shows that the critical zones are in accordance with the experimental results of Fig. 12. However, Tsai-Wu failure index is a measure of possible composite failure under static loads. To extend the life expectation of the wheel over a reasonable number of cycles, the design of the wheel is tailored to keep the failure index under a reasonable value. The effective fatigue life of the wheel will be then verified within the experimental test.

Though the experimental observations show some superficial and aesthetic damages only, a significant stiffness reduction is encountered throughout the cornering fatigue test. Fig. 14 illustrates the bending stiffness (S^*) of the composite wheel, normalised to the stiffness at the beginning of the test. The dashed line indicates the gradient at which the stiffness diminishes. A moving average filter over 30 data points has been employed to mitigate the measurement noise.

The stiffness reduction is ascribed to:

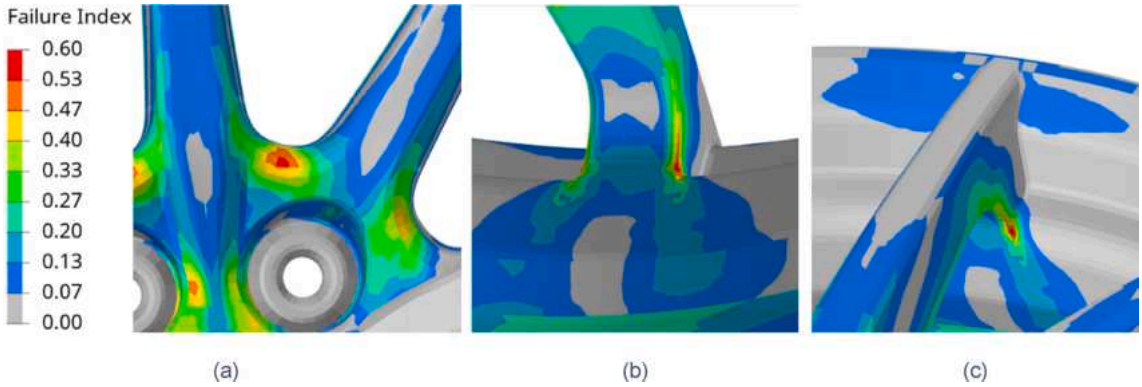

Fig. 13. Failure index evaluated for the composite wheel equipped to the 488 Pista, at the radius between two spokes (a) and between one spoke and the rim (b) inside view and (c) outside view.

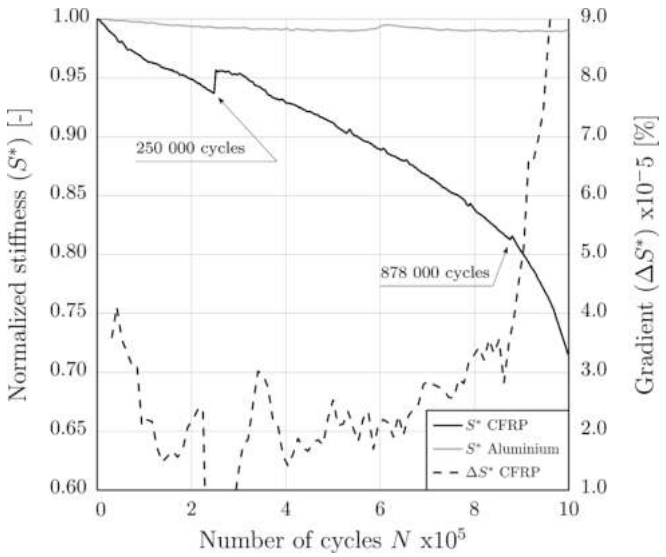

Fig. 14. Normalized stiffness (S^*) reduction during the cornering fatigue of the wheels.

1. inherent *stiffness degradation* of the materials (i.e. composites, foam,..) which is extensively studied in the literature [47,48]. This degradation effect is evaluated by the gradient of the stiffness reduction (ΔS^*) curve plot. In fact, the gradient stiffness curve shows higher values at the beginning and at the final stage of the test, whereas it exhibits lower values through the central part of the test;
2. cracks in the internal preform;
3. loss of tightening torque of the bolts.

It is worth to note that the S^* of the CFRP wheel decreases with a constant and appreciable rate, as the test goes on. This same behaviour cannot be perceived in the cornering fatigue test on the reference aluminium wheel. In fact, the S^* of the aluminium wheel remains above 0.9 until a crack onsets on one spoke, causing a sudden collapse of the wheel.

The progressive failure of the composite wheel may be monitored with a specific sensor, which may alert the driver in sufficient advance with respect to the wheel's failure. This aspect cannot be monitored in any aluminium wheel, as the failure mechanism is too rapid.

Furthermore, the stiffness reduction of the composite wheel may be slowed down by working on the preform, as well as on the wheel design and stacking sequence, and improving the plies-preform adhesion.

After the CT scans, the torque of the bolts has been brought back to the initial condition, thus a partial recovery of the stiffness is found as a discontinuity of the stiffness curve, e.g. Fig. 14 at 250000 cycles and at 878000 cycles when the wheel deflection was below 20% of initial deflection.

The first inspection of the wheel has been provided before the thermal spraying of the ceramic coating and before the machining of the bolted joints. At B-B cross-section, a porosity of about 4 mm is detected within the preform, no additional damages have been observed.

The second inspection has been performed after 250000 cycles in accordance with the OEM standard (see Table 1). The CT analysis revealed some cracks in the preform. A 7 mm crack insisted at the interface between laminate and preform (A-A section). In Section B-B, a crack appears from the back of the spoke and propagates for around 15 mm. On top of that, the preform seems debonding from the outer laminate. In Section C–C, two further cracks have been observed in the preform connecting the composite laminate to bolts housing. The cracks, labelled as *a* and *b* in Fig. 15, are about 9 mm and 15 mm long. Crack *b* propagates with a C-shaped path hindered by the metal insert at the bolted area.

The third inspection has been carried out at 878000 cycles when the S^* of the wheel had decreased by 20%. This value is a lower threshold adopted in many standards. From the CT scan, the crack already present in the A-A section propagates up to 22 mm through the whole width of the spoke. A new crack onsets at the outer aesthetic skin of the wheel. Moving to section B-B, the original crack bifurcates within the preform reaching the maximum extent of 42 mm. In section C–C, additional cracks occur in the preform. One of these, labelled as *c*, onsets close to crack *a*. A further crack, named *d*, exhibits two inclined branches forming a symmetric bifurcation. The *Y*-shaped branches extend by 42 mm, while its root is 14 mm long.

The test has been interrupted after 1 million cycles when the S^* decrease was about 30%. The tomography evidenced a new 19 mm long crack in section A-A which starts at the radiused root of the spoke. At section B-B, a third crack of 51 mm generates from the interface between the preform and the laminate, right at the onset of the pre-existing crack. The red circles in Fig. 15 highlight further damages inside the laminate at the outer skin of the spokes. They occur at the overlap between stacked plies which cover the preform. Finally, in section C–C, a new crack named *e*, appears between two bolted housings. Its length is 30 mm.

The cracks in the inner preform are mainly due to manufacturing defects in the preform and incorrect adhesion between the preform and the plies. Refining the manufacturing of the preform, as well as calibrating the resin transfer moulding parameters would most likely reduce these failure events, and therefore the reduction of S^* throughout the test.

4. Conclusions

This work presents a comparative fatigue analysis of an aluminium wheel and a composite wheel for a sports car. The aluminium wheel is obtained by forging and flow-forming of an Al 6082-T6 alloy. The composite wheel is manufactured from a preform made by randomly oriented short carbon fibres and polyurethane foam. The preform is coupled with unidirectional and plain weave carbon fibre plies, embedded into epoxy matrix injected via RTM. This technology is suitable to reduce the costs of a large production. Plus, the preform may be produced with short fibres obtained from the recycle of other production waste, thus reducing the overall environmental impact of the production cycle.

Numerical simulations of the cornering fatigue test evidenced the regions of these wheels where failure is more likely to occur. The first region is the fillet between the roots of two spokes, which was also detected in the literature. The second region is at the intersection between the spoke and the rim.

The composite wheel experienced a constant decrease in stiffness during the cornering fatigue test. Computerized Tomography scans of the composite wheel show the advance of fatigue cracks in the material. Some of these cracks originate from some defects which are due to the manufacturing of the preform. A careful study on the process parameters used to manufacture the preform would reduce these defects, and therefore the wheel's stiffness decrease.

A careful fail-safe dimensioning led to the design of two wheels which were able to complete a radial fatigue and a cornering fatigue

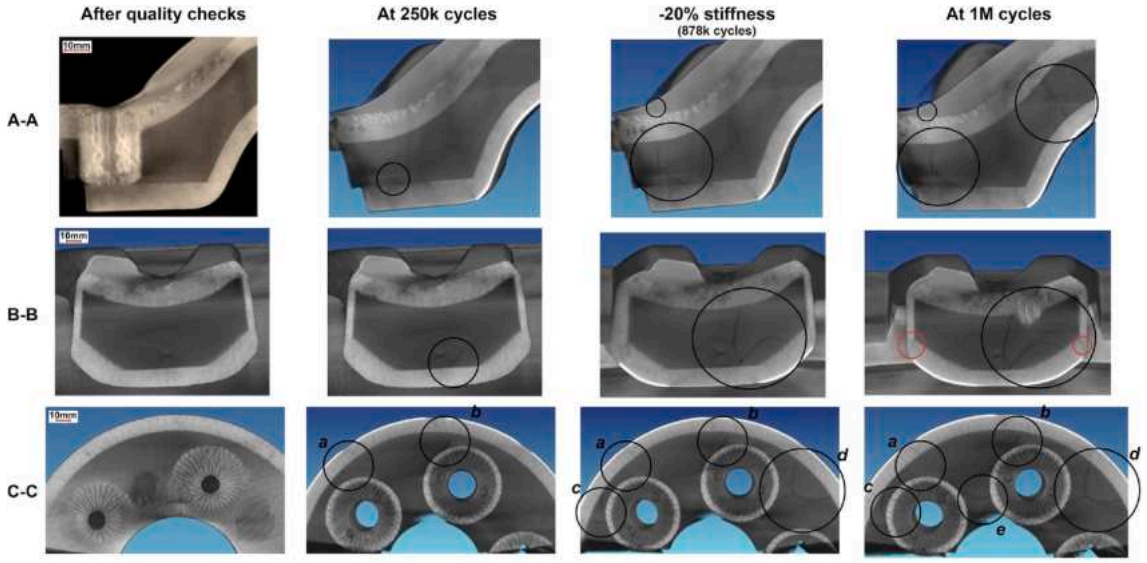

Fig. 15. CT results of the composite wheel induced by the cornering fatigue test at different cycles.

test, satisfying both the standard regulations and Ferrari protocols. In addition, results show that the cornering fatigue test leads to higher stresses on the wheel than the radial fatigue test. Hence, if a wheel successfully passes a cornering fatigue test, it is most likely to pass the radial fatigue test as well.

The new composite wheel is 28% lighter in mass than a reference forged aluminium wheel rim adopted for a similar car. Furthermore, the composite wheel is stiffer up to 8% and able to withstand loads 34% higher than the reference.

The new design is promising for the high-volume production of a new class of reliable, more efficient wheels for sports cars.

Funding

This research did not receive any specific grant from funding agencies in the public, commercial, or not-for-profit sectors.

Declaration of Competing Interest

The authors declare that they have no known competing financial interests or personal relationships that could have appeared to influence the work reported in this paper.

Data availability

The data that has been used is confidential.

Acknowledgements

The author would like to thank Carbon Revolution for their technical support on composite wheel investigation.

References

[1] G. Leister, Passenger car tires and wheels: Development - manufacturing - application, Springer. International. Publishing (2018), https://doi.org/10.1007/978-3-319-50118-5.
[2] J. Kinstler, The Science and Methodology of SAE Wheel Fatigue Test Specifications, SAE. Trans. 114 (2005) 816–826. https://www.jstor.org/stable/44718964.
[3] SAE J328:2021 Wheels - Passenger Car and Light Truck Performance Requirements and Test Procedures, SAE Technical Papers. (2021). https://doi.org/10.4271/J328_202107.
[4] ISO 3006:2015 Road vehicles — Passenger car wheels for road use — Test methods, ISO Standard. (2015).
[5] JIS D 4103:2015 Automobile parts - Wheels - Performance requirements and marking, Japanese Industrial Standard. (2015).
[6] GB/T 5334-2005 Performance requirements and test methods of passenger car wheels, National Standard of the People's Republic of China. (2005).
[7] ECE R124. Regulation No 124 of the Economic Commission for Europe of the United Nations (UN/ECE) — Uniform provisions concerning the approval of wheels for passenger cars and their trailers., (2006).
[8] SAE J2562:2021 Biaxial Wheel Fatigue Test, SAE Technical Papers. (2021).
[9] V. Grubisic, G. Fischer, Automotive Wheels, Method and Procedure for Optimal Design and Testing, SAE. Trans. 92 (1983) 508–525. https://www.jstor.org/stable/44644390.
[10] V. Grubisic, G. Fischer, Procedure for optimal lightweight design and durability testing of wheels, Int. J. Veh. Des. 5 (1984) 659–671.
[11] F. Ballo, R. Frizzi, G. Mastinu, D. Mastroberti, G. Previati, C. Sorlini, Lightweight Design and Construction of Aluminum Wheels, in: SAE Technical Papers, SAE International, 2016. https://doi.org/10.4271/2016-01-1575.
[12] R. Shang, W. Altenhof, H. Hu, N. Li, Rotary fatigue analysis of forged magnesium road wheels, Int. J. Mater. Manuf. 1 (2009) 9–15, https://doi.org/10.2307/26282629.
[13] P.R. Raju, B. Satyanarayana, K. Ramji, K.S. Babu, Evaluation of fatigue life of aluminium alloy wheels under bending loads, Fatigue. Fract. Eng. Mater. Struct. 32 (2009) 119–126, https://doi.org/10.1111/j.1460-2695.2008.01316.x.
[14] L. Wang, Y. Chen, C. Wang, Q. Wang, Fatigue life analysis of aluminum wheels by simulation of rotary fatigue test, Strojniski. Vestnik/J. Mech. Eng. 57 (2011) 31–39, https://doi.org/10.5545/sv-jme.2009.046.
[15] M. Firat, U. Kocabicak, Analytical durability modeling and evaluation-complementary techniques for physical testing of automotive components, Eng. Fail. Anal. 11 (2004) 655–674, https://doi.org/10.1016/j.engfailanal.2003.05.018.
[16] U. Kocabicak, M. Firat, Numerical analysis of wheel cornering fatigue tests, Eng. Fail. Anal. 8 (2001) 339–354, https://doi.org/10.1016/S1350-6307(00)00031-5.
[17] X. Wang, X. Zhang, Simulation of dynamic cornering fatigue test of a steel passenger car wheel, Int. J. Fatigue. 32 (2010) 434–442, https://doi.org/10.1016/j.ijfatigue.2009.09.006.
[18] Z.G. Zheng, T. Sun, X.Y. Xu, S.Q. Pan, S. Yuan, Numerical simulation of steel wheel dynamic cornering fatigue test, Eng. Fail. Anal. 39 (2014) 124–134, https://doi.org/10.1016/j.engfailanal.2014.01.021.
[19] A. Dey, H. Jugade, V. Jain, M. Adhikary, Cracking phenomena in automotive wheels: An insight, Eng. Fail. Anal. 105 (2019) 1273–1286, https://doi.org/10.1016/j.engfailanal.2019.01.069.
[20] S. Bhattacharyya, M. Adhikary, M.B. Das, S. Sarkar, Failure analysis of cracking in wheel rims - material and manufacturing aspects, Eng. Fail. Anal. 15 (2008) 547–554, https://doi.org/10.1016/j.engfailanal.2007.04.007.
[21] Z. Zheng, S. Yuan, T. Sun, S. Pan, Fractographic study of fatigue cracks in a steel car wheel, Eng. Fail. Anal. 47 (2015) 199–207, https://doi.org/10.1016/j.engfailanal.2014.09.010.
[22] M. Carboni, S. Beretta, A. Finzi, Defects and in-service fatigue life of truck wheels, Eng. Fail. Anal. 10 (2003) 45–57, https://doi.org/10.1016/S1350-6307(02)00036-5.
[23] M.M. Topaç, S. Ercan, N.S. Kuralay, Fatigue life prediction of a heavy vehicle steel wheel under radial loads by using finite element analysis, Eng. Fail. Anal. 20 (2012) 67–79, https://doi.org/10.1016/j.engfailanal.2011.10.007.
[24] E. Bonisoli, C. Rosso, S. Venturini, D. Rovarino, M. Velardocchia, Improvements on Design and Validation of Automotive Steel Wheels, in: Mechanisms and Machine Science, Springer Science and Business Media B.V, 2019, pp. 1639–1649, https://doi.org/10.1007/978-3-030-20131-9_162.
[25] M. Firat, R. Kozan, M. Ozsoy, O.H. Mete, Numerical modeling and simulation of wheel radial fatigue tests, Eng. Fail. Anal. 16 (2009) 1533–1541, https://doi.org/10.1016/j.engfailanal.2008.10.005.

[26] P.R. Raju, B. Satyanarayana, K. Ramji, K.S. Babu, Evaluation of fatigue life of aluminum alloy wheels under radial loads, Eng. Fail. Anal. 14 (2007) 791–800, https://doi.org/10.1016/j.engfailanal.2006.11.028.
[27] L. Chen, S. Li, H. Chen, D.M. Saylor, S. Tong, Study on the design method of equal strength rim based on stress and fatigue analysis using finite element method, Adv. Mech. Eng. 9 (2017), https://doi.org/10.1177/1687814017692698.
[28] K. Archibald, W. Lee, R. Rotundo, M. Melara, J. Gorsegner, C. Au, Development of a biaxial fatigue load file to emulate the services demanded of a motor sport vehicle, in: SAE Technical Papers, SAE International, 2012. https://doi.org/10.4271/2012-01-0798.
[29] D. Shang, X. Liu, Y. Shan, E. Jiang, Research on the stamping residual stress of steel wheel disc and its effect on the fatigue life of wheel, Int. J. Fatigue. 93 (2016) 173–183, https://doi.org/10.1016/j.ijfatigue.2016.08.020.
[30] P. Li, D.M. Maijer, T.C. Lindley, P.D. Lee, A through process model of the impact of in-service loading, residual stress, and microstructure on the final fatigue life of an A356 automotive wheel, Mater. Sci. Eng. A 460–461 (2007) 20–30, https://doi.org/10.1016/j.msea.2007.01.076.
[31] J. Hu, L.X. Du, J.J. Wang, Q.Y. Sun, Cooling process and mechanical properties design of hot-rolled low carbon high strength microalloyed steel for automotive wheel usage, Mater. Des. 53 (2014) 332–337, https://doi.org/10.1016/j.matdes.2013.07.036.
[32] W.F. Milliken, D.L. Milliken, Race car vehicle dynamics, Society of Automotive Engineers, 1995.
[33] F.H. Froes, D. Eliezer, E. Aghion, The science, technology, and applications of magnesium, JOM. 50 (1998) 30–34, https://doi.org/10.1007/s11837-998-0411-6.
[34] M. Zanchini, D. Longhi, S. Mantovani, F. Puglisi, On the ride comfort effect of unsprung mass reduction using a Composite Wheel Rim, in: The International Conference of IFToMM ITALY, 2022: pp. 282–289. https://doi.org/10.1007/978-3-031-10776-4_33.
[35] F. Lei, R. Qiu, Y. Bai, C. Yuan, An integrated optimization for laminate design and manufacturing of a CFRP wheel hub based on structural performance, Struct. Multidiscip. Optim. 57 (2018) 2309–2321, https://doi.org/10.1007/s00158-017-1861-7.
[36] G. Anandraj, V. Chaudhari, S. Kangde, A Comprehensive Study on the Design and Development Methodology of Automotive Steel Wheel Rims Undergoing Highly Transient Cornering Events, in: SAE Technical Papers, SAE International, 2021. https://doi.org/10.4271/2021-01-0827.
[37] Y. Zhang, Y. Shan, X. Liu, T. He, An integrated multi-objective topology optimization method for automobile wheels made of lightweight materials, Struct. Multidiscip. Optimiz. 64 (2021) 1585–1605, https://doi.org/10.1007/s00158-021-02913-3.
[38] D. Wang, S. Zhang, W. Xu, Multi-objective optimization design of wheel based on the performance of 13° and 90° impact tests, Int. J. Crashworthiness 24 (2019) 336–361, https://doi.org/10.1080/13588265.2018.1451229.
[39] J.H. Bae, K.C. Jung, S.H. Yoo, S.H. Chang, M. Kim, T. Lim, Design and fabrication of a metal-composite hybrid wheel with a friction damping layer for enhancement of ride comfort, Compos. Struct. 133 (2015) 576–584, https://doi.org/10.1016/j.compstruct.2015.07.113.
[40] X. Jiang, H. Liu, R. Lyu, Y. Fukushima, N. Kawada, Z. Zhang, D. Ju, Optimization of Magnesium Alloy Wheel Dynamic Impact Performance, Adv. Mater. Sci. Eng. 2019 (2019), https://doi.org/10.1155/2019/2632031.
[41] D. Wang, W. Xu, Y. Wang, J. Gao, Design and optimization of tapered carbon-fiber-reinforced polymer rim for carbon/aluminum assembled wheel, Polym. Compos. 42 (2021) 253–270, https://doi.org/10.1002/pc.25822.
[42] SAE J3204:2020 Aftermarket Composite Wheels Made of Matrix Material and Fiber Reinforcement Intended for Normal Highway Use - Test Procedures and Performance Requirements, (n.d.). https://doi.org/10.4271/J3204_202009.
[43] S. Aggarwal, R. Elsen, Design and Fabrication of CFRP Wheel Centre for FSAE Race-Car, in: SAE Technical Papers, SAE International, 2019. https://doi.org/10.4271/2019-28-0117.
[44] F. Rondina, S. Taddia, L. Mazzocchetti, L. Donati, G. Minak, P. Rosenberg, A. Bedeschi, E. Dolcini, Development of full carbon wheels for sport cars with high-volume technology, Compos. Struct. 192 (2018) 368–378, https://doi.org/10.1016/j.compstruct.2018.02.083.
[45] W. Chai, X. Liu, Y. Shan, X. Wan, E. Jiang, Research on simulation of the bending fatigue test of automotive wheel made of long glass fiber reinforced thermoplastic considering anisotropic property, Adv. Eng. Softw. 116 (2018) 1–8, https://doi.org/10.1016/j.advengsoft.2017.11.004.
[46] A.P. Vassilopoulos, T. Keller, Fatigue of Fiber-reinforced Composites, 2011. https://doi.org/10.1007/978-1-84996-181-3.
[47] A.P. Vassilopoulos, Fatigue Life Prediction of Composites and Composite Structures, 2020.
[48] K.L. Reifsnider, A. Talug, Analysis of fatigue damage in composite laminates, Int. J. Fatigue. 2 (1980) 3–11, https://doi.org/10.1016/0142-1123(80)90022-5.
[49] P. Alam, D. Mamalis, C. Robert, C. Floreani, C.M.Ó. Brádaigh, The fatigue of carbon fibre reinforced plastics - A review, Compos. B. Eng. 166 (2019) 555–579, https://doi.org/10.1016/j.compositesb.2019.02.016.
[50] T. Fujii, F. Lin, Fatigue Behavior of a Plain-Woven Glass Fabric Laminate under Tension/Torsion Biaxial Loading, J. Compos. Mater. 29 (1995) 573–590, https://doi.org/10.1177/002199839502900502.
[51] S.W. Tsai, E.M. Wu, A General Theory of Strength for Anisotropic Materials, J. Compos. Mater. 5 (1971) 58–80, https://doi.org/10.1177/002199837100500106.
[52] K. Dang Van, G. Cailletaud, J. Flavenot, A. le Douaron, H.P. Lieurade, Criterion for high cycle fatigue failure under multiaxial loading, in: M.W. Brown, K. J. Miller (Eds.), Biaxial and Multiaxial Fatigue, EGF 3, Mechanical Engineering Publications, London, 1989, pp. 459–478.
[53] K. Dang Van, B. Griveau, O. Message, On a new multiaxial fatigue limit criterion: theory and application, in: M.W. Brown, K.J. Miller (Eds.), Biaxial and Multiaxial Fatigue EGF 3, Mechanical Engineering Publications, London, 1989: pp. 479–496.
[54] SAE J175:2021 Wheels - Lateral Impact Test Procedure - Road Vehicles, (n.d.). https://doi.org/10.4271/J175_202107.
[55] AK-LH08:2006 Räder Anforderungen und Prüfungen, Arbeitskreis Lastenheft, Arbeitskreis der Firmen: Audi AG, Bayerische Motorenwerke AG, DaimlerChrysler AG, Porsche AG, Volkswagen AG., (n.d.).
[56] Q. Gao, Y. Shan, X. Wan, Q. Feng, X. Liu, 90-degree impact bench test and simulation analysis of automotive steel wheel, Eng. Fail. Anal. 105 (2019) 143–155, https://doi.org/10.1016/j.engfailanal.2019.06.097.
[57] G. Previati, F. Ballo, M. Gobbi, G. Mastinu, Radial impact test of aluminium wheels—Numerical simulation and experimental validation, Int. J. Impact. Eng. 126 (2019) 117–134, https://doi.org/10.1016/j.ijimpeng.2018.12.002.
[58] C.L. Chang, S.H. Yang, Simulation of wheel impact test using finite element method, Eng. Fail. Anal. 16 (2009) 1711–1719, https://doi.org/10.1016/j.engfailanal.2008.12.010.
[59] F. Ballo, G. Previati, G. Mastinu, F. Comolli, Impact tests of wheels of road vehicles: A comprehensive method for numerical simulation, Int. J. Impact. Eng. 146 (2020), https://doi.org/10.1016/j.ijimpeng.2020.103719.
[60] X. Wan, X. Liu, Y. Shan, E. Jiang, H. Yuan, Numerical and experimental investigation on the effect of tire on the 13° impact test of automotive wheel, Adv. Eng. Softw. 133 (2019) 20–27, https://doi.org/10.1016/j.advengsoft.2019.04.005.
[61] J. Stearns, T.S. Srivatsan, A. Prakash, P.C. Lam, Modeling the mechanical response of an aluminum alloy automotive rim, Mater. Sci. Eng. A 366 (2004) 262–268, https://doi.org/10.1016/j.msea.2003.08.017.
[62] X. Wan, Y. Shan, X. Liu, H. Wang, J. Wang, Simulation of biaxial wheel test and fatigue life estimation considering the influence of tire and wheel camber, Adv. Eng. Softw. 92 (2016) 57–64, https://doi.org/10.1016/j.advengsoft.2015.11.005.
[63] F.M. Santicolli, R. Möller, I. Krause, F.G. Dedini, Simulation of the scenario of the biaxial wheel fatigue test, Adv. Eng. Softw. 114 (2017) 337–347, https://doi.org/10.1016/j.advengsoft.2017.08.006.
[64] M. Biancalana, M. Zanchini, Wheel rim of a vehicle, EP3650243, 2021.
[65] G. Goldoni, S. Mantovani, Damage modelling strategies for unidirectional laminates subjected to impact using CZM and orthotropic plasticity law, Compos. Struct. 275 (2021), https://doi.org/10.1016/j.compstruct.2021.114493.
[66] Y. Zhou, D. Jiang, Y. Xia, Tensile mechanical behavior of T300 and M40J fiber bundles at different strain rate, J. Mater. Sci. 36 (2001) 919–922, https://doi.org/10.1023/A:1004803202658.
[67] N.S. El-Tayeb, R.M. Gadelrab, A.W. Profe, Friction and wear properties of E-glass fiber reinforced epoxy composites under different sliding contact conditions, Wear 192 (1996) 112–117, https://doi.org/10.1016/0043-1648(95)06770-1.
[68] A.J. Denmead, M.D. Silcock, T. Corbett, S. Agius, B. Trippit, Shaped Preform for Face Portion of a Composite Wheel, WO/2019/033173, 2019.

[69] M. Holmes, High volume composites for the automotive challenge, Reinf. Plast. 61 (2017) 294–298, https://doi.org/10.1016/j.repl.2017.03.005.
[70] L. de Lorenzis, F. Grancagnolo, A. L'Erario, A. Maffezzoli, A. Miccoli, S. Rella, M. Spedicato, G. Zavarise, Analysis and Characterization of the Mechanical Structure for the I-Tracker of the Mu2e Experiment, Nucl. Phys. B. Proc. Suppl. 248–250 (2014) 134–136, https://doi.org/10.1016/j.nuclphysbps.2014.02.027.
[71] K. Kluger, Fatigue life estimation for 2017A–T4 and 6082–T6 aluminium alloys subjected to bending-torsion with mean stress, Int. J. Fatigue. 80 (2015) 22–29, https://doi.org/10.1016/j.ijfatigue.2015.05.005.
[72] S. Mantovani, I. lo Presti, L. Cavazzoni, A. Baldini, Influence of Manufacturing Constraints on the Topology Optimization of an Automotive Dashboard, Procedia Manuf. 11 (2017) 1700–1708. https://doi.org/10.1016/j.promfg.2017.07.296.
[73] F. Ballo, M. Gobbi, G. Mastinu, G. Previati, Motorcycle tire modeling for the study of tire-rim interaction, J. Mech. Des. Trans. ASME. 138 (2016), https://doi.org/10.1115/1.4032470.
[74] R.G. Pelle, FEM simulation of the tire/rim seating process, Tire. Sci. Technol. 22 (1994) 76–98, https://doi.org/10.2346/1.2139537.